Contents lists available at ScienceDirect

Petroleum Science

journal homepage: www.keaipublishing.com/en/journals/petroleum-science



Original Paper

Deblending by sparse inversion and its applications to highproductivity seismic acquisition: Case studies



Shao-Hua Zhang a, *, Jia-Wen Song b

- ^a China National Petroleum Corporation, Beijing, 100007, China
- b BGP INC., CNPC, Baoding, 072750, Hebei, China

ARTICLE INFO

Article history: Received 20 December 2024 Received in revised form 8 March 2025 Accepted 17 March 2025 Available online 20 March 2025

Edited by Meng-Jiao Zhou

Keywords: Deblending Sparse inversion Simultaneous sources High-productivity Seismic acquisition

ABSTRACT

Deblending is a data processing procedure used to separate the source interferences of blended seismic data, which are obtained by simultaneous sources with random time delays to reduce the cost of seismic acquisition. There are three types of deblending algorithms, i.e., filtering-type noise suppression algorithm, inversion-based algorithm and deep-learning based algorithm. We review the merits of these techniques, and propose to use a sparse inversion method for seismic data deblending. Filtering-based deblending approach is applicable to blended data with a low blending fold and simple geometry. Otherwise, it can suffer from signal distortion and noise leakage. At present, the deep learning based deblending methods are still under development and field data applications are limited due to the lack of high-quality training labels. In contrast, the inversion-based deblending approaches have gained industrial acceptance. Our used inversion approach transforms the pseudo-deblended data into the frequency-wavenumber-wavenumher (FKK) domain, and a sparse constraint is imposed for the coherent signal estimation. The estimated signal is used to predict the interference noise for subtraction from the original pseudo-deblended data. Via minimizing the data misfit, the signal can be iteratively updated with a shrinking threshold until the signal and interference are fully separated. The used FKK sparse inversion algorithm is very accurate and efficient compared with other sparse inversion methods, and it is widely applied in field cases. Synthetic example shows that the deblending error is less than 1% in average amplitudes and less than -40 dB in amplitude spectra. We present three field data examples of land, marine OBN (Ocean Bottom Nodes) and streamer acquisitions to demonstrate its successful applications in separating the source interferences efficiently and accurately.

© 2025 The Authors. Publishing services by Elsevier B.V. on behalf of KeAi Communications Co. Ltd. This is an open access article under the CC BY-NC-ND license (http://creativecommons.org/licenses/by-nc-nd/

1. Introduction

With the shift of hydrocarbon exploration to more complex areas, such as deep-buried reservoirs in desert, mountainous regions, or deep oceans, wide-azimuth and high-density 3D seismic acquisition gradually emerged in the late 1990's (Lynn, 1996; Li, 1999) and early 2000's (Vermeer, 2002; Quigley, 2004), respectively. It is because wide-azimuth and high-density seismic acquisition can improve the signal to noise (S/N) ratio, resolution, and imaging quality of seismic data, laying the foundation for better subsequent subsurface characterization than conventional acquisition. Consequently, it leads to an increasing need to reduce the

cost of seismic data acquisition yet without compromising the accuracy and fidelity of seismic data. Indeed, wide-azimuth and highdensity seismic start to gain the acceptance of the industry due to the advent of high-productivity seismic acquisition technology until the early 2010's (Zhang and Zhan, 2021; Zhang and Song,

Traditionally, seismic sources are deployed with sufficient time interval, or when a source completes its sweep at one shot location, it then moves to the next shot location together with the receiver spread. Obviously, the efficiency of this shot-by-shot fashion is low, and cannot satisfy the needs of wide-azimuth and high-density seismic acquisition. The bottle neck for improving efficiency here is the source and receiver waiting time, and reducing waiting time is a basic strategy to improve the efficiency. It intuitively requires the deployment of multiple sources which sweep in different modes with millions of receiver channels and without the need to

E-mail address: zhangshhua@cnpc.com.cn (S.-H. Zhang).

^{*} Corresponding author.

relocate the spread.

In marine seismic data acquisition, Berkhout (2008) proposed the concept of simultaneous shooting with random time delays, signalling the onset of blended seismic acquisition (Hampson et al., 2008). In land seismic data acquisition, Shell proposed alternative sweep in 1991, and slip sweep in 1996 (Rozemond, 1996). It is followed by distance-separated slip sweep and dynamic slip sweep, which was widely applied in the Middle East and North African (Bouska, 2008). BP developed Independent Simultaneous Sweeping (ISS) technique in 2006 and applied it in Libya project in 2008 (Howe et al., 2009; Abma et al., 2015). On the above-mentioned basis, BGP developed the UHP (ultra-high-productivity) sweep in 2018 which employs more source groups and large receiver spreads, further optimizing the sweep timing and modes (Zhao et al., 2018).

The use of these high-productivity acquisition methods substantially reduces the field operation time, making wide azimuth and high-density surveys economically feasible. However, the recorded wavefield is no longer clean compared with traditional surveys, and the acquired data are contaminated with interferences generated from adjacent source groups, referred to as being blended. Therefore, accurate deblending is required before subsequent data processing, which is the extra price paid for high-productivity acquisition.

Initially, deblending was treated as a noise suppression process utilizing various filtering techniques (e.g., Mahdad et al., 2011; Zhou et al., 2013). Then, deblending was treated as an inversion process (Song et al., 2019a, 2019b) with priors. Nowadays, deblending based on deep-learning is also gradually emerged (e.g., Wang et al., 2022, 2023a; Chen, 2024). We review and discuss the merits of these various deblending techniques in order to provide a good understanding of these techniques and facilitate a useful discussion on how these deblending techniques can help high-productivity seismic acquisition.

Note that another approach is to process the blended data directly without deblending. Dai et al. (2011) and Verschuur and Berkhout (2011) applied reverse time migration (RTM) directly to blended data. Zhang et al. (2018) carried out full wave inversion (FWI) of blended data directly. However, both RTM and FWI require an initial velocity model with sufficient accuracy to produce meaningful results. Due to the limitation in computing capacity, such models were often produced from the deblended data before the application of RTM or FWI, which made this approach impractical.

In this paper, after a review of the published deblending techniques, we propose to use a sparse inversion method for seismic data deblending with synthetic data to demonstrate its accuracy. Three field data examples of land, marine OBN (Ocean-Bottom-Nodes) and streamer geometries are further provided to illustrate its role in high-productivity onshore and offshore seismic acquisitions.

2. Deblending techniques

Deblending is a data processing procedure to separate the source interferences of blended data from simultaneous sources with random time delays. The separated data can then be processed using the traditional seismic data processing procedures. Deblending approach has attracted wide interests from the industry and academia in recent years. Generally speaking, there are three categories of deblending algorithms: filtering-type deblending approaches, deterministic inversion based deblending approaches, and deep learning based deblending approaches. The development of these techniques is reviewed below.

2.1. Filtering-based deblending algorithm

If a blended dataset is acquired from simultaneous sources with random time delays, the useable data (or the signals) from the main shot are coherent and continuous, whilst the interferences (the blending noise) from adjacent shots appear random and discontinuous (Beasley, 2008) in CRP (common-receiver-point), or CMP (common-mid-point), or COG (common-offset-gather) data domains instead of the common-shot-point (CSP) domain. The filtering approach exploits this feature to separate the signals from the blending noise using conventional random noise removal techniques, of which median filter and its various modifications were first proposed (e.g., Liu et al., 2009; Huo et al., 2012; Gan et al., 2016; Zhou and Li, 2018, amongst others).

Liu et al. (2009) was amongst the first to introduce the traditional scalar median filter to separate the interference noise in pseudo-deblended data. Doulgeris et al. (2011) and Mahdad et al. (2011) introduced a coherence filter in the *f-k* domain to remove the interference noise. Meanwhile, Huo et al. (2012) extended the traditional scalar media filter to a vector media filter for deblending in CMP domain, and Wang et al. (2014) further improved this approach with an additional trim-threshold to maximize the energy of the main shot.

However, the separated results by these filtering techniques were often not very satisfactory due to the presence of residual noise. In order to remove the residual noise, multi-domain and iterative filtering techniques are developed. Han et al. (2013) suggested to remove the interference noise by median filter in the COG domain first, and then further filtering is applied in the curvelet domain to remove the residual energy. Gan et al. (2016) proposed a structure-oriented median filtering technique. The data was first aligned along a selected horizon (or structure), and then a median filter was applied for deblending. Zhou et al. (2016a) introduced an iterative approach which adjusts the filtering time window self-adaptively during each iteration, and the median filtering was repeated with an updated time window until the residual energy meets the pre-set threshold.

Apart from median filters, there are also other noise suppression techniques, like tau-p transform (Zhang and Olofsson, 2012). In recent years, Lin et al. (2022) developed a robust singular-value spectra analysis (SSA) algorithm for deblending each frequency segment of the pseudo-deblended data. Dong et al. (2021) developed a singular value decomposition method (SVD) for deblending in CMP domain after normal moveout correction. Whilst Wilson et al. (2023) shifted the focus from the random interfering noise to the coherent signals, and developed a coherency filter to estimate the signal for subtraction from the pseudo-deblended data. The residual data was then input to the coherency filter for signal estimation and subtraction. This process is repeated until no-more coherent signal can be detected in the residual data.

However, due to limitations of these various noise-removing techniques, such as filtering assumptions and the parameter selection restrictions (like filtering type and window length), there is often a lack of sufficient separation accuracy. In particular, when the blending fold (i.e., number of simultaneous sources) is high, and the signal-to-noise ratio (S/N) is low, the filtering-based deblending approach may result in both signal distortion and noise leakage (Song et al., 2019a). As a result, more advanced techniques were actively implemented in commercial high-productivity seismic data acquisitions, despite these filtering-based deblending techniques are often computational efficient.

2.2. Inversion-based deblending algorithm

Following Berkout (2008), the blended data in common-

receiver-point (CRP) domain can be written as

$$d = \Gamma m \tag{1}$$

where d represents the blended data, m represents the desired unblended data in CRP domain, i.e., the signal model, and Γ is the blending operator which contains the shooting times and positions of all sources. Eq. (1) implies that we can consider a blended seismic acquisition as a forward modelling process. Therefore, deblending may be considered as the inverse of the blended acquisition, that is,

$$m = \Gamma^{-1}d, \tag{2}$$

where Γ^{-1} is the inverse of Γ , if it exists.

As we know, in conventional unblended acquisition, a receiver records each source separately. Whilst in a blended acquisition, the receiver records multiple sources simultaneously. Therefore, there are more variables in the signal model m than those in the blended data d, and Γ is not a square matrix. Thus, the inverse of Γ does not exist. Note that a square matrix is a necessary condition for the matrix inversion, and another condition is non-singular. Furthermore, the inversion problem of Eq. (2) is underdetermined and illposed. To solve such a problem, it requires some prior knowledges or assumptions of the signal. Commonly, the first step in solving such problems is to compute the conjugate transpose of Γ , denoting as $\Gamma^{\rm H}$, which can be considered as an approximation of Γ^{-1} . Thus, pseudo-deblended data m_P can be achieved:

$$m_{\rm P} = \Gamma^{\rm H} d. \tag{3}$$

Apart from introducing the concept of pseudo-deblended data, the other common assumption is the sparsity of the signal in a particular transform domain to constrain the inversion problem (e.g., Zhou et al., 2016b; Li et al., 2019). Various sparse transforms have been used for blended data separation, including Fourier transforms (Abma et al., 2010), Radon transform (Ibrahim and Sacchi, 2014), seislet transform (Chen et al., 2014), curvelet transform (Qu et al., 2016; Cao et al., 2019), and dictionary learning (Zu et al., 2018), etc.

The main differences amongst different inversion algorithms are the choices of sparse transforms and regularization constrains (i.e., L_0 , L_1 -or L_2 -norm), which leads to some hybrid approaches. For example, Chen et al. (2014) and Chen (2015) introduced an iterative scheme with multiple constrains via seislet domain shaping regularization. Qu et al. (2016) combined curvelet transform with different regularization constrains, and Cao et al. (2019) combined curvelet transform with focal transform for blended data deblending. Meanwhile, Zu et al. (2018) proposed an iterative deblending scheme based on a combination of hybrid sparse transforms with dictionary learning. Besides, low rank assumption is also used during deblending (Cheng and Sacchi, 2015).

Compared with the filtering-based deblending methods, the above inversion methods have improved the deblending accuracy. However, their computational cost is too high to be adopted in commercial seismic acquisition activity. Particularly, they are not applicable during UHP (ultra-high-productivity) and USS (unrestricted simultaneous shooting) seismic acquisition. In this case, the blending fold and data volume are both very high, and the S/N ratio may be very low (Song et al., 2019a). Furthermore, for both filtering- and inversion-based deblending approaches, the choices of super-parameters such as window length, type of transforms and signal or noise threshold are very subjective and empirical. These parameters often need to be determined by trial and error, and are not transferable between different datasets.

To tackle these issues and to improve the accuracy and

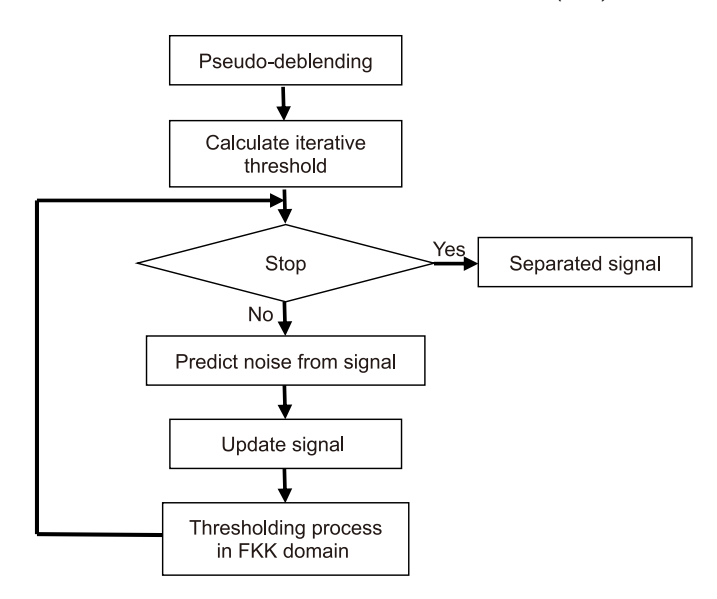


Fig. 1. The workflow of the FKK sparse inversion method for deblending.

generality of deblending algorithms, Song et al. (2019a, 2019b) developed a sparse inversion method in the frequency-wavenumber-wavenumber (FKK) domain for accurate, robust and efficient deblending. It has been verified in subsequently commercial operations (Li et al., 2019; Song et al., 2020) and it works in common-receiver gathers. The method processes the FKK spectra with a hard exponential shrinking threshold function to accelerate the convergence. Moreover, the computation efficiency is further enhanced by Fast Fourier Transform (FFT) and parallel computing as receivers are mutual independent.

2.3. Deep-learning based deblending algorithm

As artificial intelligence (AI) gains momentum, deep-learning based deblending started to appear in the literature (e.g., Baardman and Hegge, 2020; Sun et al., 2020; Zu et al., 2020; Wang et al., 2021).

Initially, the focus was on the use of supervised learning for deblending. For example, Baardman and Hegge (2020) was amongst the first to introduce supervised learning to detect and attenuate blending noise. Sun et al. (2020) introduced the convolutional neuron network (CNN) and Zu et al. (2020) constructed a deep neuron network (DNN) to supress the blending noise. However, supervised learning requires large quantities of unblended data as training datasets, and such data are often not available in reality, which restricts the applications of supervised deblending techniques (Wang et al., 2021). Therefore, there is a need to reduce the dependence of deep learning-based technique on labelled training datasets in order to improve their capacity for practical application.

Thus, deblending based on self-supervised or un-supervised learning provides a possible solution (Chen, 2024). One approach is to use the pseudo-deblended data (m_P) in the CSP domain as training data to achieve self-supervised learning for CRG deblending. For example, Xu et al. (2022) used the m_P in CSP domain to train a convolutional auto-encoder for deblending. Whilst Chen and Wang (2023) proposed first to use the m_P in the CSP domain as training datasets, then performed a multi-step training and verification, and finally applied the optimized network to pseudo-deblended data in CRP domain.

Another approach is to use synthetic data for training, such as in the case of Birnie and Alkhalifah (2022). They first used the synthetic data to train a supervised blind-spot network, and its weights

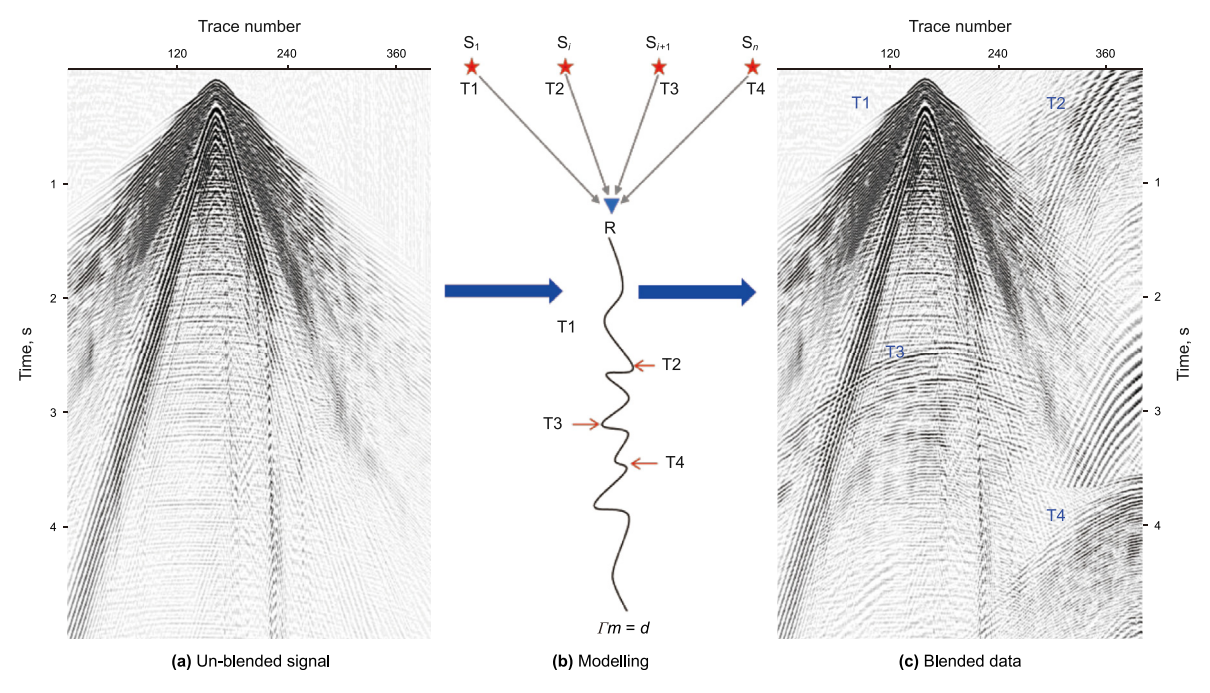


Fig. 2. Synthetic data example: (a) An unblended CSP gather; (b) mathematic model of the blending process; (c) the pseudo-deblended CSP gather.

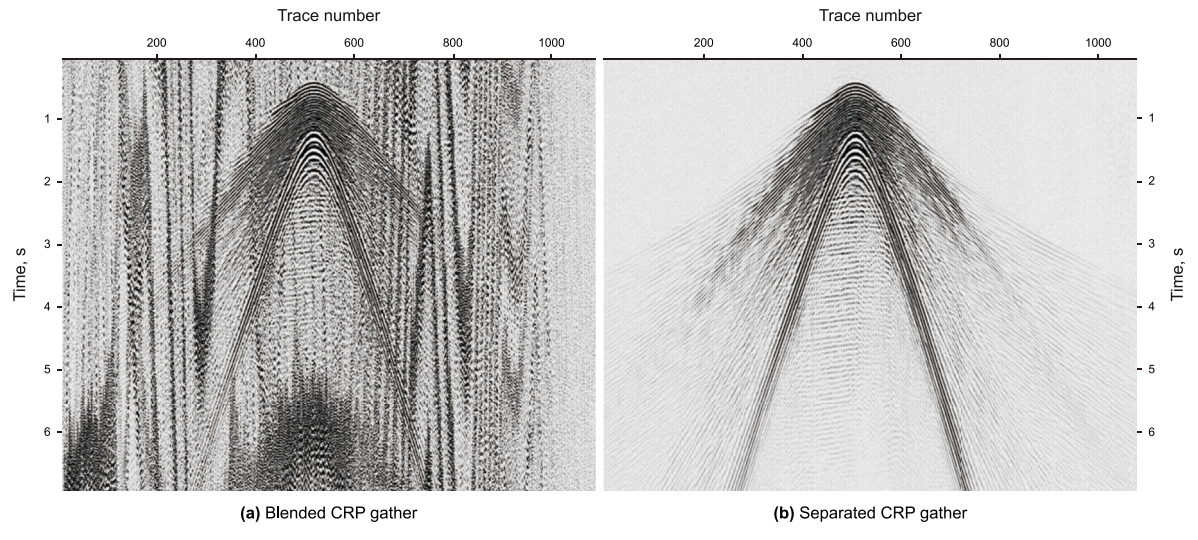


Fig. 3. Synthetic data example: (a) A pseudo-deblended CRP gather; (b) the deblended CRP gather.

were then used to initialize a self-supervised blind-spot network. Moreover, transfer learning is used to improve the network's ability for noise suppression and signal protection. The blind-spot network originates from image processing (Laine et al., 2019) and Wang et al. (2023b) named this blind-spot network as blind-trace network, and developed a similar self-supervised learning scheme. It opens a new approach for self- or un-supervised deep learning (e.g., Luiken et al., 2023; Wang et al., 2024).

Despite the above efforts, there is still a considerable gap for deep learning techniques to achieve practical commercial applications.

3. The FKK sparse inversion method

Sparse inversion is a commonly used approach to solve underdetermined geophysical inversion problems, such as pre-stack or post-stack seismic sparse inversion. In this approach, the sparsity of the desired results is assumed, and an objective function is introduced based on different sparse norm regularizations (L_0 , L_1 or L_2). Then, the desired result can be obtained via minimizing the objective function. In this way, the inverse problem is converted to an optimization problem. Here, the same strategy is used for seismic deblending.

3.1. Methodology and workflow

To solve Eq. (1), we assume the 3D signal m is sparse in the model space, and it is applicable in either space-time domain or frequency-wavenumber-wavenumber (FKK) domain. We impose the L_0 -norm constraint on the FKK spectrum of the signal m, and the objective function J(m) for optimization can be written as

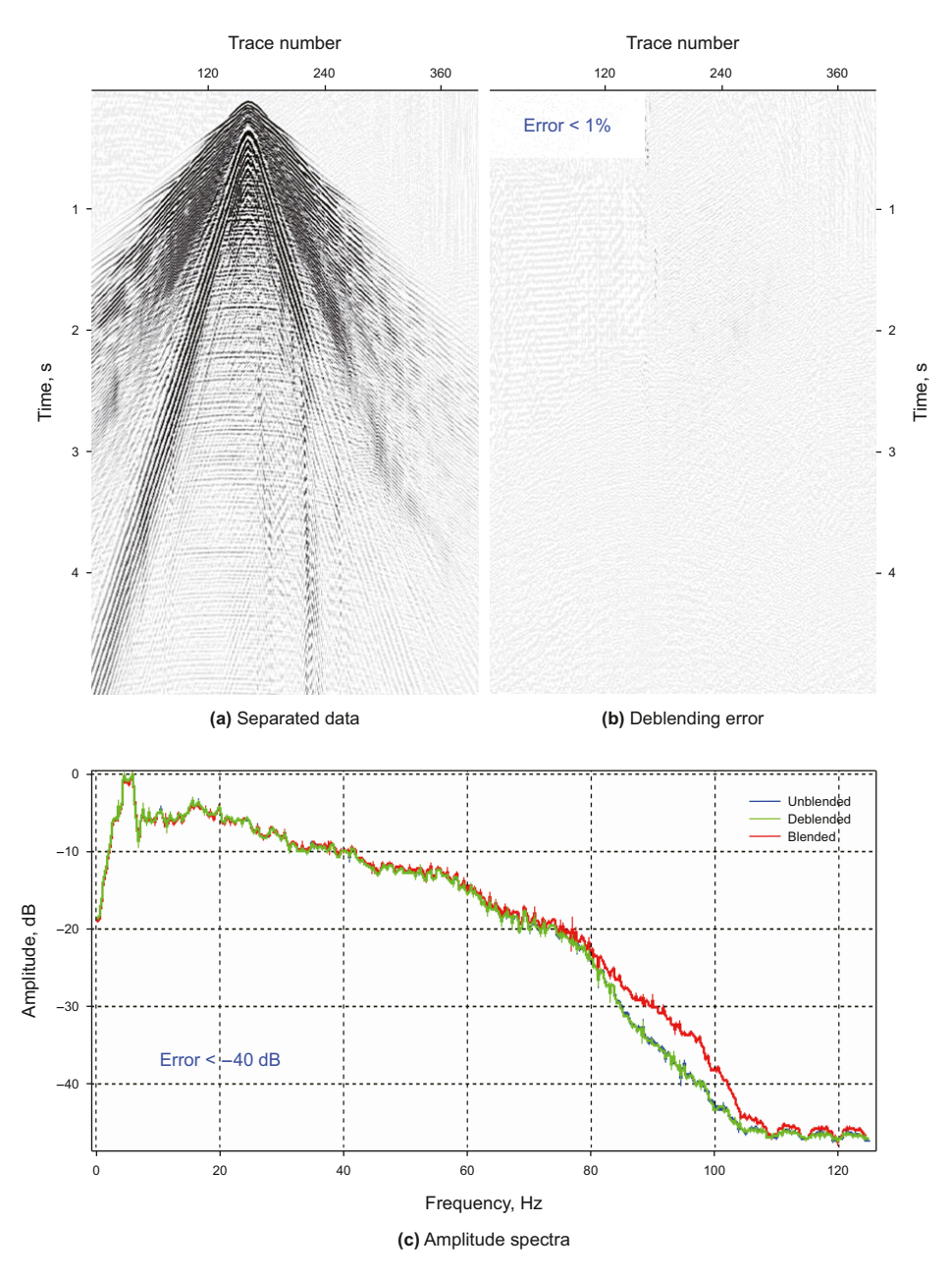


Fig. 4. Synthetic data example: (a) the deblended CSP gather; (b) the deblending residual between the deblended results in (a) and the original unblended signal in Fig. 2(a); (c) amplitude spectra comparison of the unblended signal (blue), deblended data (green), and the pseudo-deblended data (red).

$$J(m) = \|d - \Gamma m\|_2^2 + \lambda \|Fm\|_0, \tag{4}$$

where F denotes the 3D forward Fourier transform operator and λ is the regularization parameter that controls the weights of the constraint. For Fourier coefficients sparse constraints, Eq. (4) can be rewritten as

$$\begin{cases} J(x) = \|d - Lx\|_{2}^{2} + \lambda \|x\|_{0} \\ x = Fm \\ L = \Gamma F^{-1} \end{cases}, \tag{5}$$

where F^{-1} is the 3D inverse Fourier transform operator. Note that Eq. (5) is a standard optimization problem with objective function

J(x), and the desired solution x can be solved by a standard iterative shrinking threshold algorithm (Daubechies et al., 2004; Blumensath and Davies, 2008):

$$x_{i+1} = T_{\tau} \left[x_i + L^{\mathsf{H}} (d - L x_i) \right], \tag{6}$$

where T_{τ} is the thresholding operator in the transform domain (FKK), and L^{H} is the conjugate transpose of L. Substituting the expressions of x and L in Eq. (5) into Eq. (6) gives

$$m_{i+1} = F^{-1}T_{\tau}F\left[\Gamma^{\mathsf{H}}d - \left(\Gamma^{\mathsf{H}}\Gamma - I\right)m_{i}\right],\tag{7}$$

where I is the identity matrix. The term $\Gamma^{H}d$ is the pseudo-deblended CRP gather as defined in Eq. (3), and $(\Gamma^{H}\Gamma - I)m_{i}$



(a) A land vibroseis acquisition

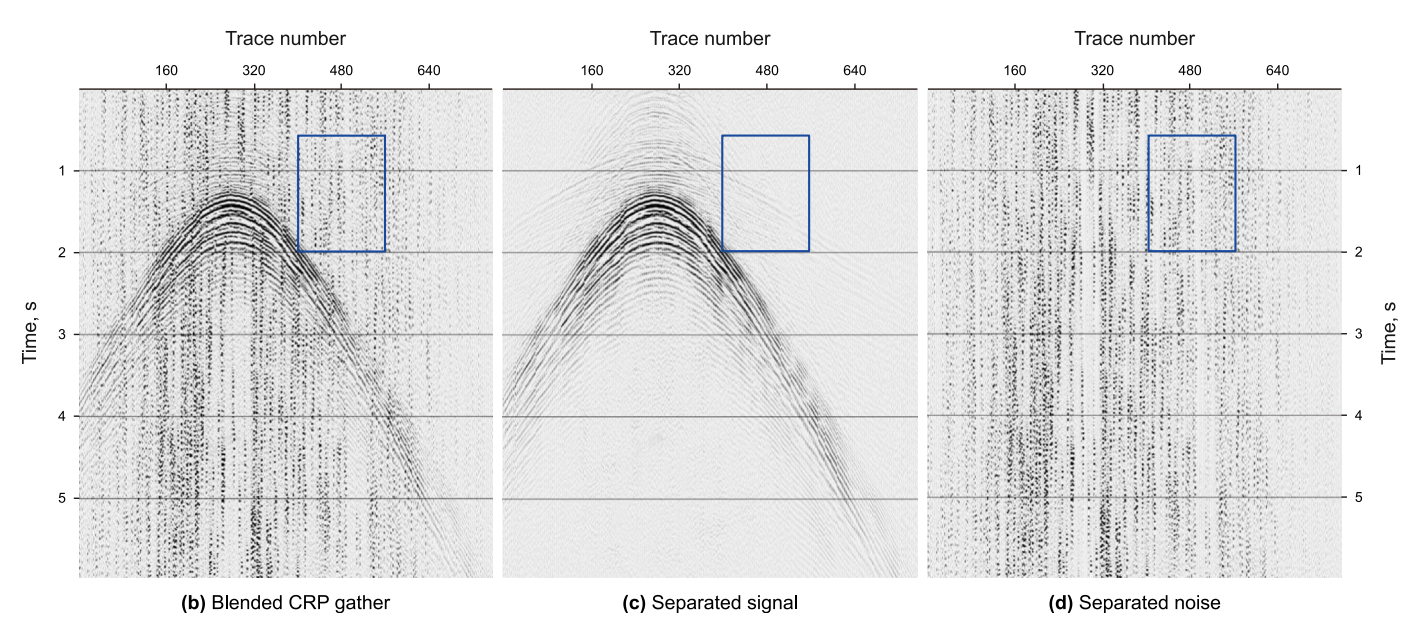


Fig. 5. (a) A land vibroseis acquisition, (b) pseudo-deblended data, (c) extracted signal and (d) separated noise. The deblended results are obtained by the FKK sparse inversion (Song et al., 2019a) in CRP gathers.

represents the interference noise predicted by the estimated signal. Note that the initial signal m_0 is typically set to zero. Here, in order to reduce uncertainties during iterative deblending, we adopt a hard thresholding function to set the coefficients to zero when their amplitudes are less than the given threshold:

$$T_{\tau}[f(m)] = \begin{cases} f(m), |f(m)| \ge \tau \\ 0, |f(m)| < \tau \end{cases}, \tag{8}$$

where f(m) denotes the spectrum coefficients in the FKK domain, and τ is the given threshold. To further speed up the convergence rate, the shrinking threshold function is given as

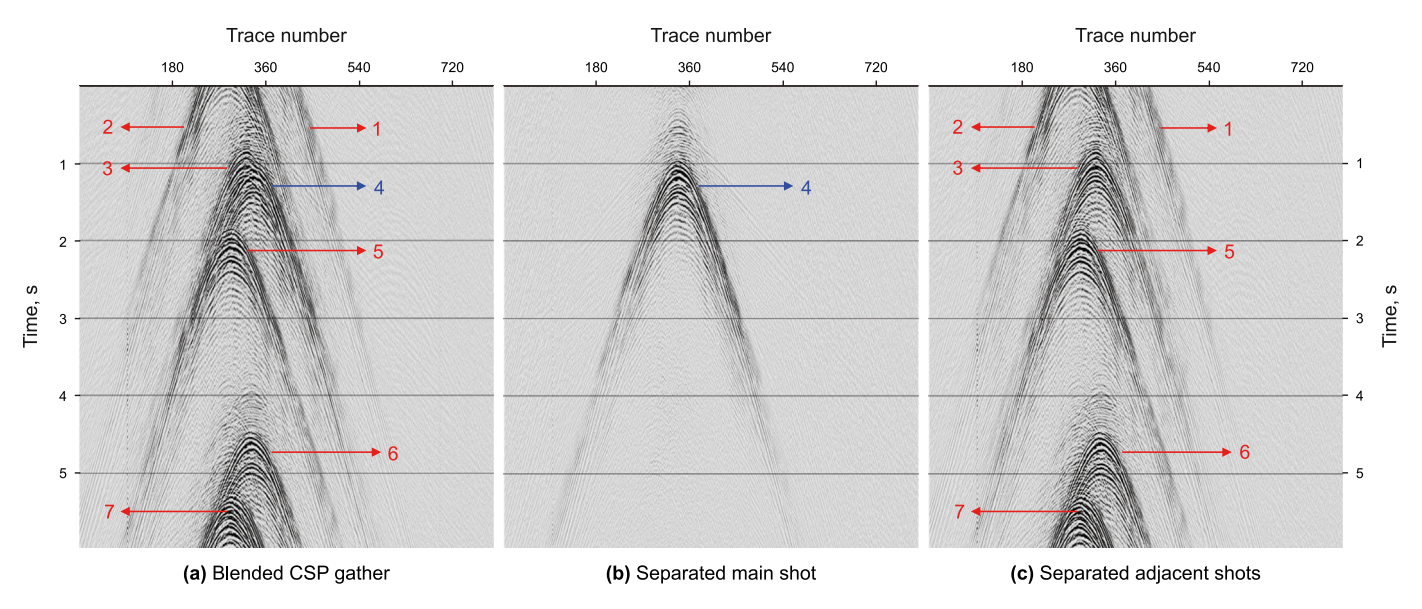


Fig. 6. The deblended results in CSP gathers by the FKK sparse inversion (Song et al., 2019a): (a) pseudo-deblended data, (b) separated main shot, and (c) separated adjacent shots.

$$\tau_k = \tau_0 * a^k, k = 1, 2, ..., N, \tag{9}$$

where τ_k is the threshold at the k-th iteration, and τ_0 is the maximum FKK coefficient of the pseudo-deblended data $m_{\rm P}$. The symbol N is the total number of iterations, and a denotes the threshold attenuation coefficient.

Fig. 1 shows the workflow of the above-mentioned deblending method. As shown in Fig. 1, there are six steps in the workflow.

- 1) Calculate the pseudo-deblended data m_P using formula $\Gamma^H d$;
- 2) Calculate the maximum FKK coefficient of the pseudo-deblended data, and determine the shrinking threshold function τ_k ;
- 3) Calculate and predict the interference noise from the initial (or updated) signal using expression $(\Gamma^{\mathsf{H}}\Gamma I)m_i$;
- 4) Subtract the predict noise from the pseudo-deblended data to update the signal using expression $\Gamma^{H}d (\Gamma^{H}\Gamma I)m_{i}$;
- 5) Apply the thresholding criteria to the FKK spectra of the signal using formula followed by inverse Fourier transform $F^{-1}T_{\tau}F[\Gamma^{\rm H}d-(\Gamma^{\rm H}\Gamma-I)m_{\rm f}];$
- 6) Repeat step 3 to step 5 until the maximum number of iterations *N* is reached to obtain the finally separated signal.

3.2. Synthetic blended data tests

We first use synthetic blended data to test the accuracy of the above-mentioned inversion method. The synthetic blended data is generated with a blending fold of 4, that is, the receiver recorded data from 4 blended sources shooting simultaneously with random time delays. The procedure to generate the blended data is shown in Fig. 2. Firstly, we select an unblended shot gather with an OBN geometry (Fig. 2(a)). Secondly, based on the positions of the 4 shots, we arrange the shot gather into 4 groups, and design the timing of the shots using the trace recording length as interval plus some random delay times. Finally, we shift the traces according to the excitation time of the corresponding shot, and sum the shifted 4 groups together to obtain the blended data and the corresponding pseudo-deblended data is shown in Fig. 2(c). As shown in Fig. 2(c), there are many interferences from the adjacent shots, which are

continuous and coherent either from the main shot, or from the adjacent shots in the CSP domain.

To apply the FKK sparse inversion method, we first transform the pseudo-deblended data from the CSP domain to the CRP domain (Fig. 3(a)). As shown in Fig. 3(a), due to random delay times of the shots, only the data from the main shot show coherent and continuous events. The interferences from the adjacent shots appear random and discontinuous, agreed with Beasley (2008). Fig. 3(b) shows the separated signal in CRP domain: the interference noise is completely removed, and the weak deep events below 5000 ms are all recovered.

To further evaluate the accuracy of the deblended data, we then transform the total deblended results from the CRP domain back to the CSP domain. We calculate the deblending residual between the deblended shot gather (Fig. 4(a)) and the original unblended shot gather (Fig. 2(a)), as shown in Fig. 4(b). There is no observable signals leakage in Fig. 4(b), and the deblending error in average amplitudes is calculated as less than 1%.

As shown in Fig. 4(c), we further calculate the amplitude spectra of the original unblended signal in Fig. 2(a) (blue curve), the deblended results in Fig. 4(a) (green curve), as well as the pseudodeblended data in Fig. 2(c) (red curve) for better comparisons. We can see that the blue and green curves completely overlap each other, and the deblending error in amplitude spectra is calculated as less than -40 dB.

Accurate deblending is the foundation for high-productivity seismic acquisition, and Figs. 3 and 4 confirm that the FKK sparse inversion can suppress the interference noise without degrading the signal, which paves the way for field data applications. Note that an exponential shrinking threshold is used and its initial value is set at the maximum amplitude of the dataset and the iteration terminates at about a thousandth of the initial threshold value. It often takes about 50–150 iterations to reach the target threshold value. This remains the same for all examples used in this paper.

3.3. Field data testing

A land dataset from Oman is used, and the dataset was specially acquired for feasibility testing of blended acquisition. Twelve vibrators were deployed with the same sweeping frequency from 1.5 to 96 Hz, as shown in Fig. 5(a), and vibrated simultaneously with

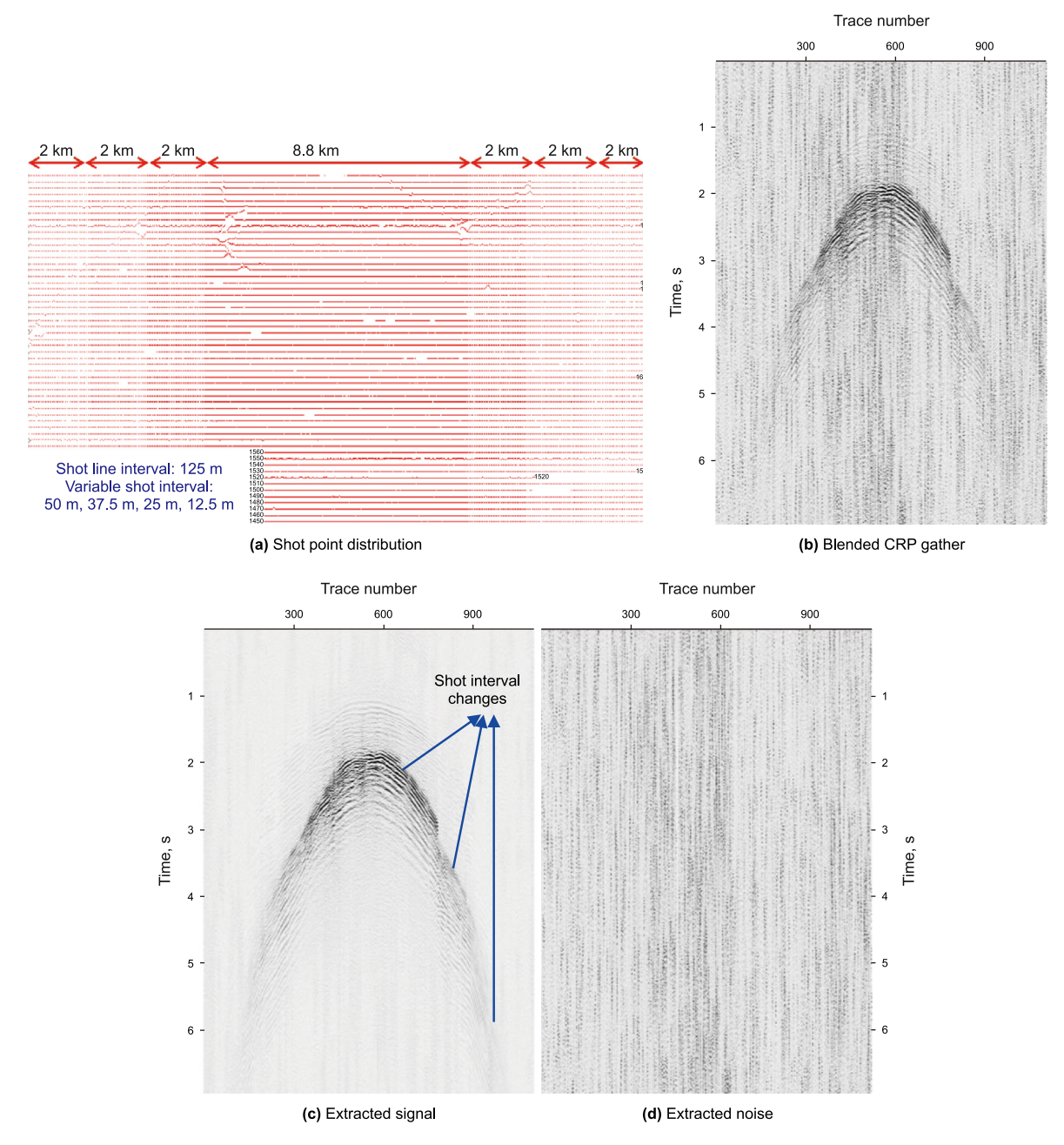


Fig. 7. Land vibroseis example: (a) shot point distribution, (b) pseudo-deblended data in CRP domain, (c) extracted signal and (d) separated noise by the FKK sparse inversion method (Song et al., 2019a).

random time delays. A fixed spread was used which consisted of 18 receiver lines and 798 receivers per line with a total of 14364 channels to continuously record of the vibrating signals. Receiver interval is 25 m and receiver line interval 250 m. There are 81 shot lines and 398 shots per line with a total of 32238 shots. The shot point interval and the shot line interval are both 25 m. The recording length is 9 s with 4 ms sampling rate.

Fig. 5(b) shows a pseudo-deblended CRP gather after cross-correlation between the recorded and sweep signals. We can see that the signals are coherent and continuous, including primary reflections and their multiples, as well as refractions and ground rolls. However, the interferences from adjacent shots are incoherent because of random shooting times. Almost all types of deblending methods exploit this distribution differences to

separate the signal from the blending noise. Fig. 5(c) shows the separated signals using the FKK sparse inversion method. We can see that all signals are well recovered, including the weak signal in the blue box. More importantly, Fig. 5(d) shows the separated noise, which shows no coherent signals and implies that there is no signal leakage, and the fidelity of the coherent events in Fig. 5(b) is well preserved.

To further examine the deblended results, we transform the total separated results from CRP domain to the CSP domain. As shown in Fig. 6(a), there are a total of seven interfering sources in the pseudo-deblended data. Note that the apices of these sources are close to each other, indicating that the spatial interval between the sources is small, which increases the deblending difficulty. The signals from the main source (shot 4) are completely recovered

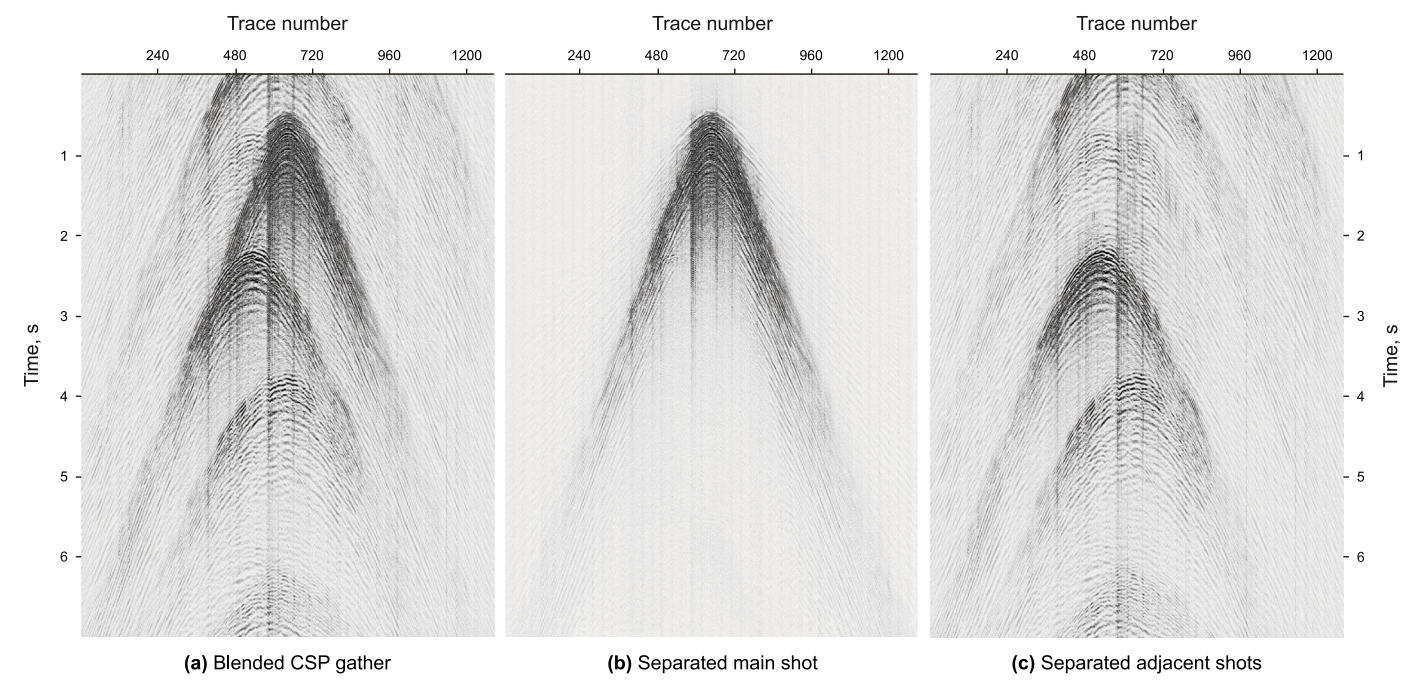


Fig. 8. Land vibroseis example: (a) pseudo-deblended data in CSP domain, (b) separated main shot, and (c) separated adjacent shots.

without any observable interferences from the other sources, as shown in Fig. 6(b). The adjacent shots are also completely recovered as shown in Fig. 6(c). In particular, except for the missing main shot, Fig. 6(c) looks exact the same as Fig. 6(a). It confirms that the FKK sparse inversion can successfully separating the signal from the blending noise without compromise the fidelity and accuracy of the signal.

4. Application examples

High-productivity blended acquisition has now become a standard practice for hydrocarbon exploration in both onshore and offshore activities. The above introduced FKK sparse inversion method has been widely applied for deblending in subsequent data processing. Here, we select three representative examples with varying deblending difficulties to illustrate its applications, including land vibroseis, marine Ocean-bottom-node (OBN), and marine streamer.

4.1. Land vibroseis case

The data are acquired by unrestricted simultaneous shooting (USS) in Egypt, and at least 30 vibrators are deployed during blended acquisition with independent simultaneous shooting (ISS) with no time-distance separation. Moreover, variable shot intervals were adopted to further improve acquisition efficiency. Fig. 7(a) shows the shot-point distribution, and the shot interval is 12.5 m in the central area measured 8.8 km wide, and gradually increases to 50 m in the two ends of the operation area. The pseudo-deblended data in the CRP domain are shown in Fig. 7(b). There is serious blending noise in Fig. 7(b) due to both the high blending fold and the USS acquisition. We can also observe the effects of changing shot interval, as marked by the blue arrows in Fig. 7(c). All these issues can degrade the performance of a majority of deblending methods. However, the FKK sparse inversion method can account for these issues and recover the signal very accurately as shown in Fig. 7(c). There is no residual noise in Fig. 7(c) and no coherent signal leakage in Fig. 7(d).

The corresponding pseudo-deblended shots, the separated main shot and adjacent shots are shown in Fig. 8(a), (b) and (c), respectively. We can see that there is no signal distortion and no leakage from the adjacent shots. Both the main shot and the adjacent shots are completely recovered (Fig. 8(b) and (c)).

Note that it is often very difficult to preserve the low and high frequency components during deblending, particularly for USS acquisition with high blending fold. Therefore, the operator specially required that all vendors should test their deblending ability for recovering the low and high frequency components. Our results are shown in Fig. 9. The low frequency content between 2 and 4 Hz is completely recovered without distortion (Fig. 9(b)). The high frequency contents between 64 and 125 Hz are shown in Fig. 9(c) and (d) before and after deblending. Comparisons between Fig. 9(a) and (b), as well as between Fig. 9(c) and (d), reveal that there is no noise leakage and no signal distortion after deblending.

USS acquisition presents the most serious challenges for data deblending in land vibroseis acquisition due to high blending fold, no time-distance separation, and variable shot intervals. Figs. 7–9 show that the FKK sparse inversion method can still separate such data with sufficient high accuracy.

4.2. Marine OBN case

Unlike blended acquisition on land, the randomness of source excitation is not ideal in a marine environment, as seismic vessels often travel at fixed routes with a constant speed. As we know, shot time variations are crucial for separating the blended data. Therefore, the source dithering time within a certain range (e.g. ± 300 ms) is usually imposed on the shot time to reduce the risk of source synchronization, and improve the randomness of the shot times. Some additional restrictions on the number of sources and distance between them may also be imposed to ensure accurate deblending. In this example, six sources from two dual-source vessels and two single source vessels were deployed in the acquisition. The dithering time is randomly perturbed within a range of ± 300 ms. The

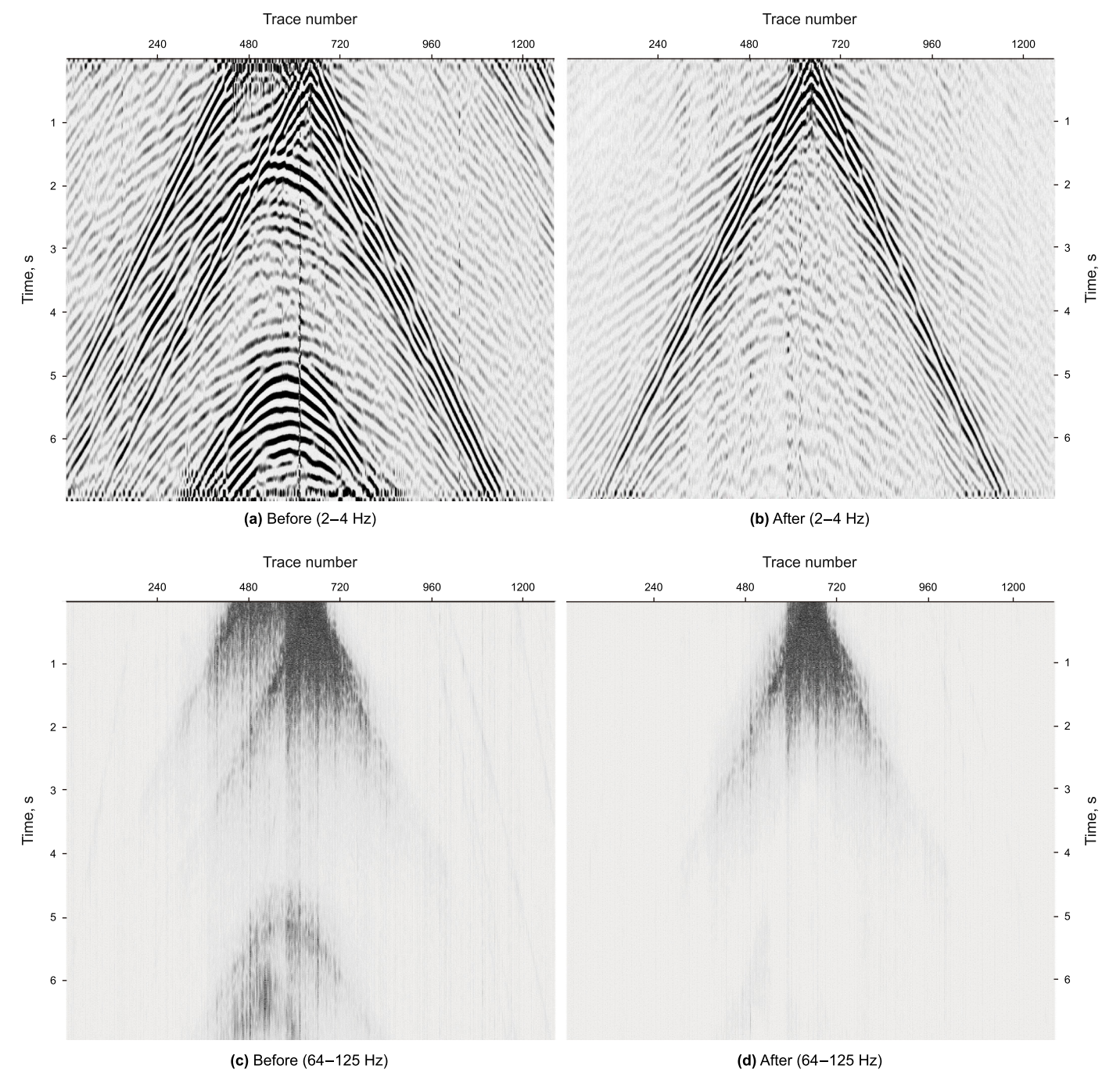


Fig. 9. Land vibroseis example: comparisons of the low frequency content between 2 and 4 Hz of the data (a) before and (b) after deblending, and comparisons of the high-frequency content between 64 and 125 Hz (c) before and (d) after deblending.

minimum separation between the boats is 6 km, but the separation of the two sources on the dual-source boats is only 50 m and does not meet this condition. It induces serious interferences between each other. Interferences from other vessels are also severe despite the requirement of minimum separation distance. Consequently, most of the deblending methods failed in the accuracy tests and the FKK sparse inversion method is one of a few methods passed the tests set up by the operator. Here, we present the performance of the FKK sparse inversion method in Figs. 10–12.

Fig. 10(a) shows the operation area of the four source vessels. The two dual-source vessels operate in areas 1 and 3, and the two

single-source vessels in areas 2 and 4. Fig. 10(b) shows the pseudo-deblended data in CRP domain, and serious interference can be seen below 5000ms. Nevertheless, the FKK method correctly recover the signal as shown in Fig. 10(c). In contrast, there is obvious remaining noise by a traditional filtering method (Wang et al., 2014) in Fig. 10(d).

Fig. 11 shows a comparison of the CSP domain data before and after deblending. The data from the main shot are marked by the blue arrow, and interferences from the same vessel are marked by red arrows, and those from the other vessels are marked by pink arrows. As shown in Fig. 11(a), all interferences show coherent

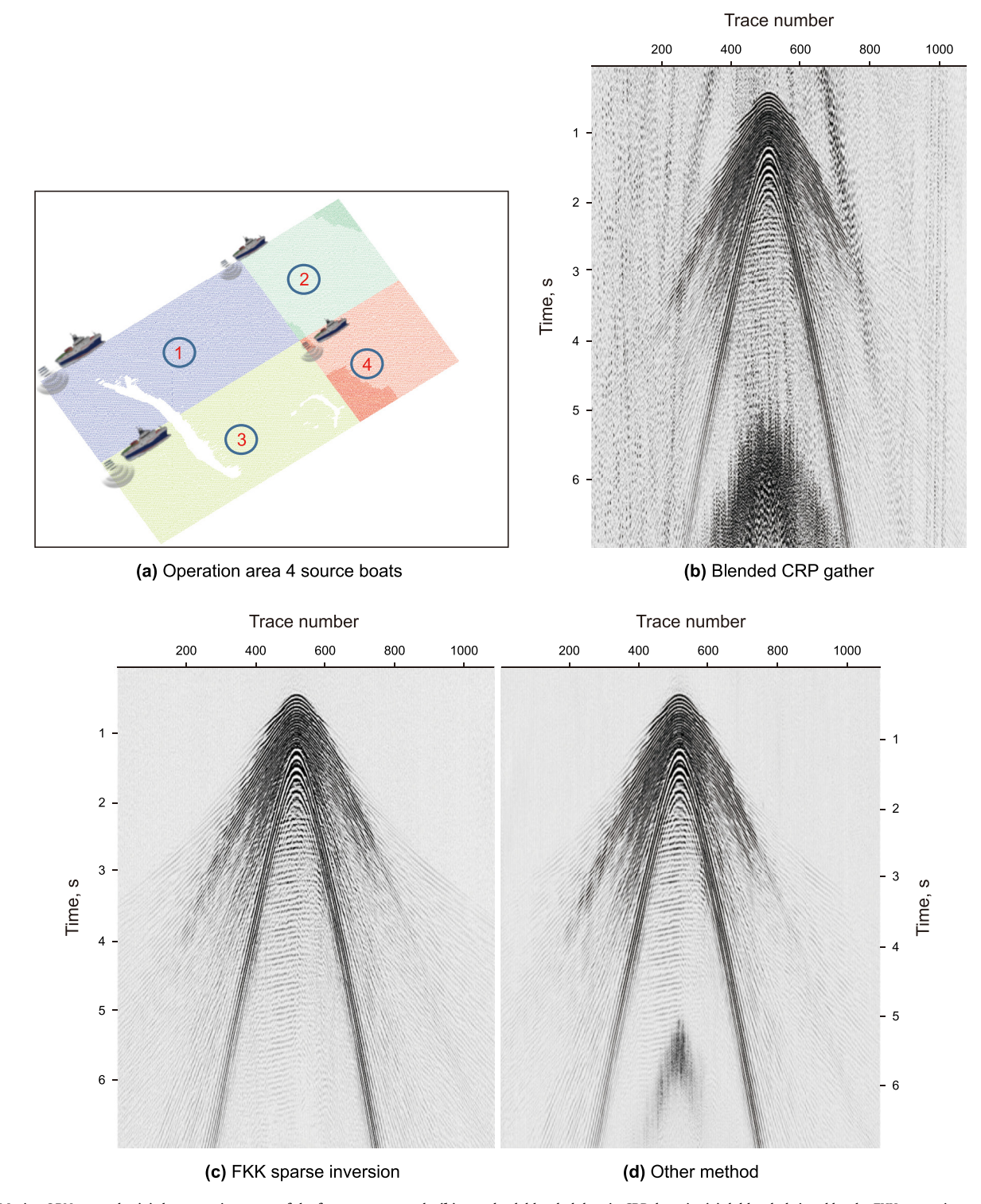


Fig. 10. Marine OBN example: (a) the operation areas of the four source vessels, (b) pseudo-deblended data in CRP domain, (c) deblended signal by the FKK sparse inversion method and (d) deblended data by a traditional filtering method (Wang et al., 2014) for comparison.

energy, and those interferences from the same vessel show similar trajectory and strong energy as the signal from the main shot which makes deblending more difficult than those interferences from the other vessels. Despite this, the FKK method still recovers the data from the main shot correctly (Fig. 11(b)).

Fig. 12 shows a comparison of the post-stack data before and after deblending in order to further demonstrate the effectiveness

of the FKK sparse inversion method. We can see serious interferences from sources of the same vessels (Fig. 12(a)) which are all removed after deblending and coherent and continuous events can be seen in Fig. 12(b), although the energy appears a little weak.

Marine OBN acquisition presents new challenges for seismic deblending due to lack of randomness in source excitation compared with land vibroseis. Figs. 10–12 confirm that the used

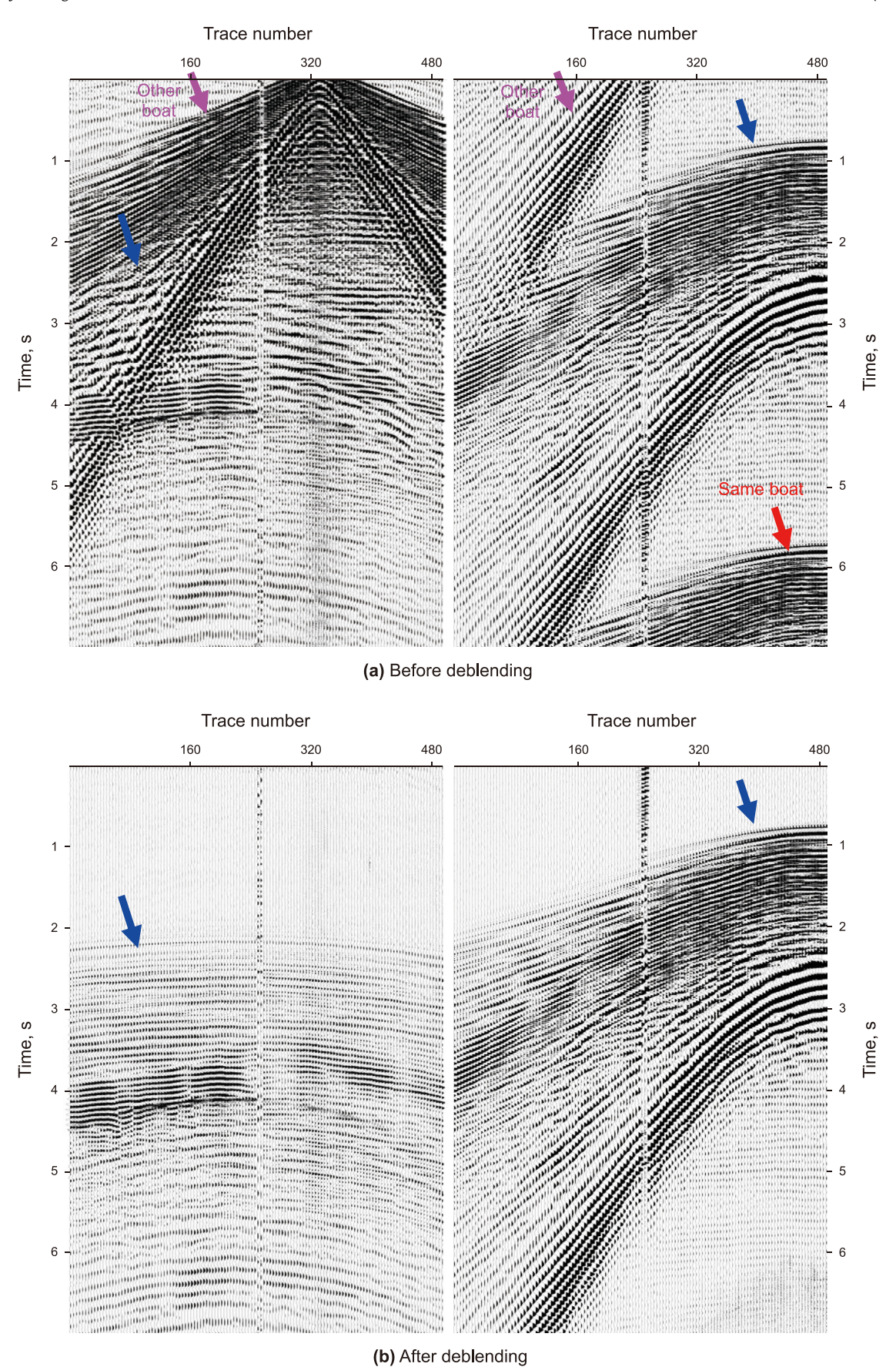


Fig. 11. Marine OBN example: comparison of CSP domain data (a) before and (b) after deblending. Blue arrows mark the data from the main shots, red and pink arrows mark the interferences from the same and other vessels, respectively.

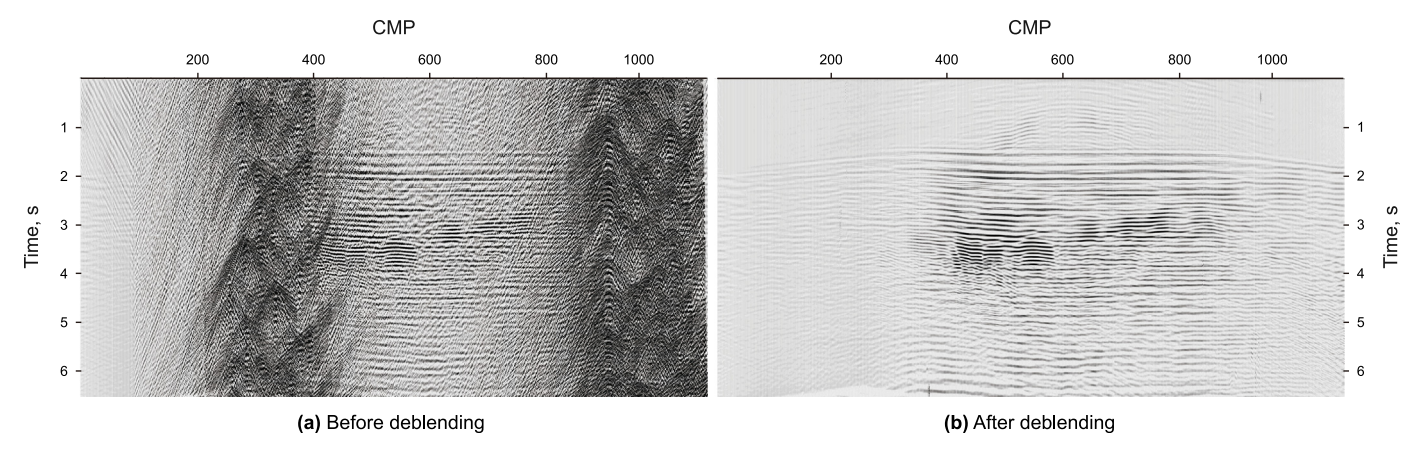


Fig. 12. Marine OBN example: comparison of post-stack sections (a) before and (b) after deblending.

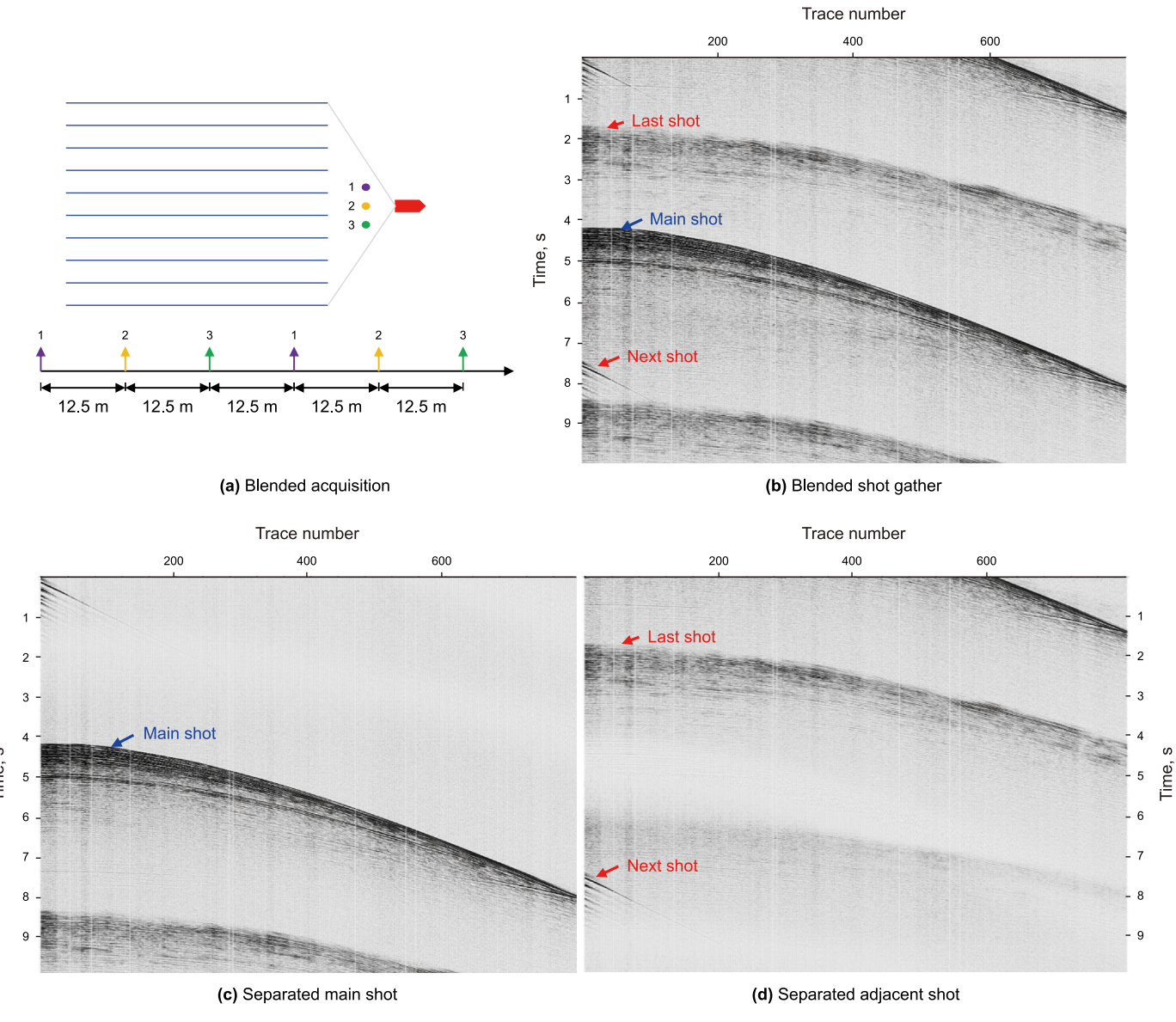


Fig. 13. (a) Configuration of three sources in a streamer vessel, referred to as the 3-source and 1-vessel case, (b) pseudo-deblended data in CSP domain, (c) separated main shot, and (d) separated adjacent shots.

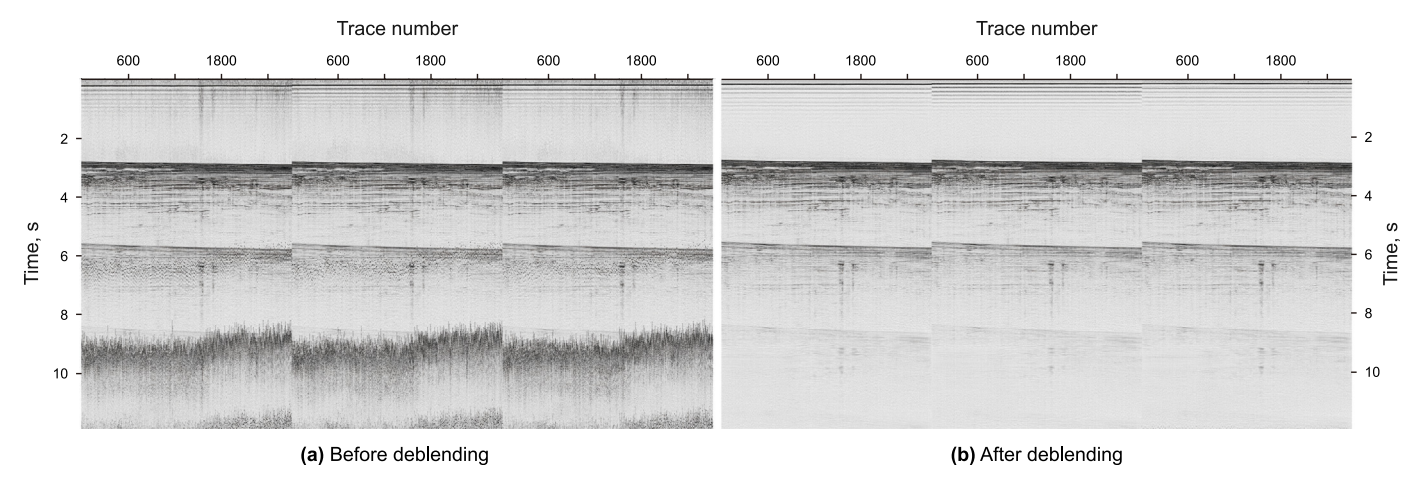


Fig. 14. The 3-source 1-vessel case: comparison of data in CRP domain (a) before and (b) after deblending.

FKK sparse inversion method can still handle such case without compromising the deblending accuracy and fidelity.

4.3. Marine towed streamer

In the previous OBN case, a combination of multiple sources in single and multiple vessels are deployed during blended seismic data acquisition. It is similar to blended towed streamer acquisition. The main difference is that there are often more sources in a streamer source vessel than an OBN source vessel. Therefore, seismic deblending is often more challenging for the streamer case than the OBN case. Here we present two cases. One uses three sources in a single vessel, referred to as the 3-source 1-vessel case (Figs. 13 and 14), and the other using six sources in three vessels, i.e., the 6-source 3-vessel case (Fig. 15), to illustrate the streamer case applications of the FKK sparse inversion method. In both cases, the distance between sources in the same vessel is 50 m, and the minimum distance between the vessels is 6 km. The source dithering time is randomly perturbed within a range of ± 250 ms in this case. The receiver interval is 12.5 m, and recording length 10 s with 4 ms as sampling interval.

Fig. 13(a) shows the configuration of the three sources in a streamer vessel, and the data from all three sources can be seen in the pseudo-deblended CSP gather in Fig. 13(b). The red arrows mark the interferences from the previous and next shots, and blue arrows mark the signal from the main shot. As we can see that the main shot and those adjacent shots are all properly separated using the FKK sparse inversion method (Fig. 13(c) and (d)).

Fig. 14 shows a comparison of the data in a CRP domain before and after deblending. The interference noises appear random and discontinuous in Fig. 14(a) and are removed completely after deblending as shown in Fig. 14(b). Note that in land or OBN acquisition, the position of a receiver is fixed, and the source-receiver distance changes as a source moves away or towards the receiver. However, in a tow-steamer acquisition, a receiver moves with the sources, and the source-receiver distance is fixed. Therefore, common-receiver gather from a towed-streamer acquisition is similar to a common-offset gather in a land or OBN acquisition.

Fig. 15 shows a comparison of the CSP domain data before and after deblending for the 6-source 3-vessel case. The red arrows mark the interferences of the adjacent shots from the two adjacent vessels, and these interferences are coherent and continuous with strong energy (Fig. 15(a)). The deblending of such data is not a simple task due to small distance between the sources on the same vessel. After several tests on the shrinking thresholds, some

gradient weights are used (Song et al., 2020) to properly separate the shots with sufficient deblending accuracy as shown in Fig. 15(b). Fig. 16 shows a comparison of a stack section before and after deblending, and it can be seen that deblending is critical for accurately imaging the subsurface. Fig. 16(a) before deblending is seriously contaminated by the noise from adjacent shots which are removed in Fig. 16(b) after deblending.

In terms of deblending, the issues in marine towed-streamer acquisition are slightly more complicated to those in the OBN case. Firstly, in both cases, there is a lack of source excitation randomness compared with land vibroseis. Secondly, the interferences from sources of the same boat are more serious in the towed-streamer case than the OBN case, since there are often more sources in a marine streamer vessel than an OBN source vessel. Regardless of a multi-source single-vessel case or a multi-source multi-vessel case, the FKK sparse inversion method can still handle these cases accurately and efficiently to provide separated results for subsequent seismic data processing and inversion.

5. Discussions

In this paper, we have reviewed the development of three types of deblending techniques, including filtering, inversion, and deep learning-based deblending algorithms. We also propose to use the FKK sparse inversion method for seismic data deblending together with its applications in high-productivity seismic acquisitions. Using synthetic blended data, we have evaluated the accuracy of the FKK deblending technique, and then present its applications in three case blended acquisitions with different acquisition geometries.

The first case is the land vibroseis, where high degree of randomness for the firing time can be achieved with high blending fold and highest productivity efficiency amongst the three cases. The second case is the marine OBN acquisition, and the degree of randomness is lower than land vibroseis due to the fixed source vessel parameters. The randomness of the blending noise mainly depends on the dithering time of the shots, which increases the deblending difficulties. Thus, in OBN acquisitions, additional restrictions such as minimum distance between source vessels need to be imposed, which reduces the acquisition efficiency to some extents. The third case is the marine steamer acquisition and further deblending difficulties arise due to close configuration of multiple sources in the same vessel. Despite these various difficulties, our deblended results have shown that the proposed FKK method can handle these situations accurately and efficiently. How

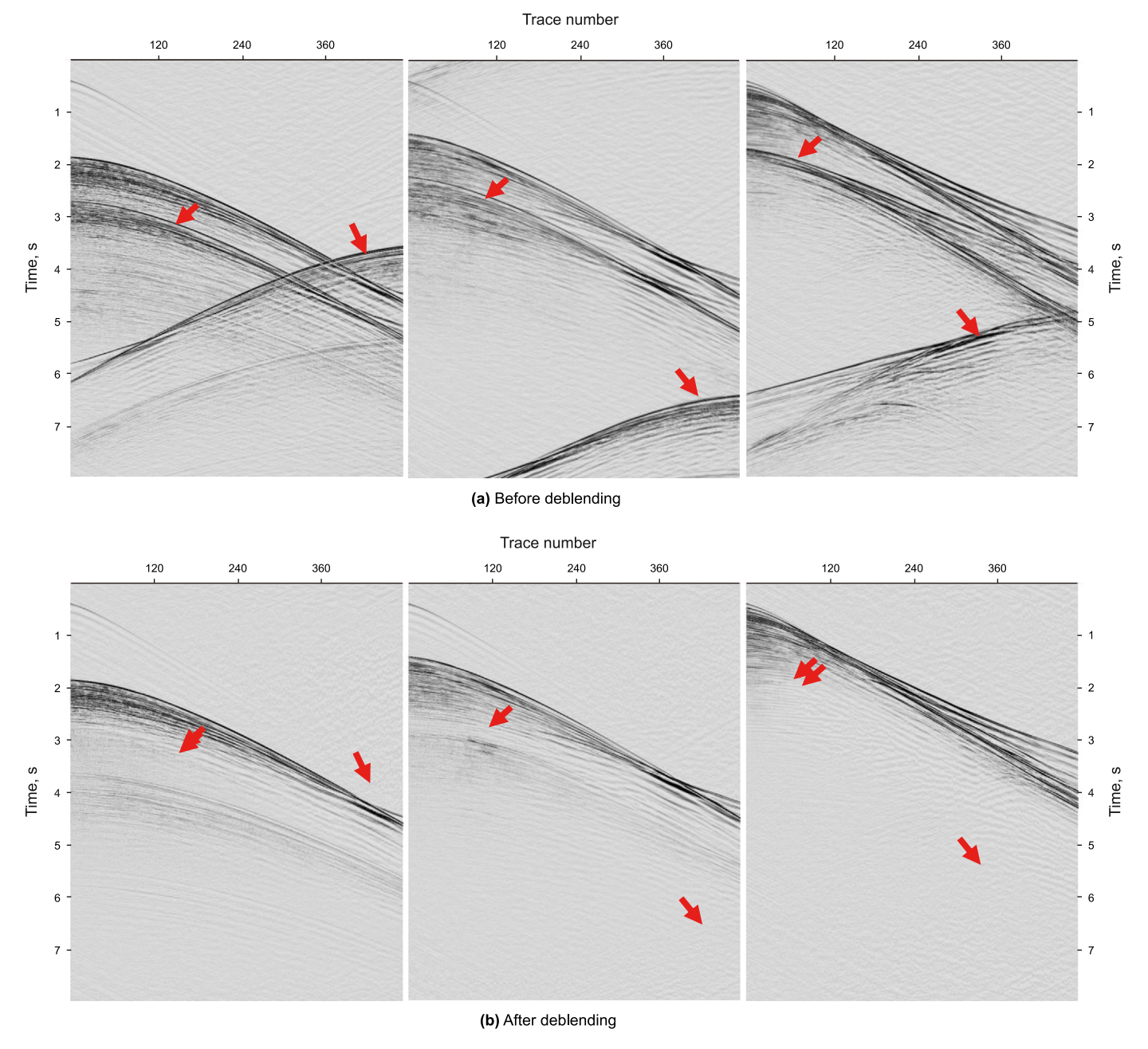


Fig. 15. The 6-source 3-vessel case: comparison of data in CSP domain (a) before and (b) after deblending. The red arrows mark the interferences of adjacent shots from the other two boats.

does the used FKK technique compare with other deblending techniques, such as, the traditional filtering-based deblending techniques? Here we give a brief discussion below.

Song et al. (2019a, 2019b) compared the deblended results using the FKK sparse inversion and the filtering-based deblending method on synthetic and field data. They conclude that the filtering-based method can only handle cases with low blending fold and simple geometries, and there is a lack of deblending accuracy in most practical cases. For a convenient comparison, Fig. 17 shows a field data example modified from Song et al. (2019a), where there are more than six blended sources present in the pseudo-deblended common source gathers (Fig. 17(a)). Harmonic noise appearance in each source before first arrivals is critical

benchmark signal for the deblending process in terms of whether these harmonic noises are accounted for properly. As shown in Fig. 17(b), the blending noise produced by harmonics have been appropriately removed. In contrast, Fig. 17(c) shows that the filtering-based deblending method fails to suppress such noise. More comparisons can be found in Song et al. (2019a, 2019b, 2020).

Currently, the deep learning methods can only be applied to artificially blended data and field blended data application is limited due to lack of training labels despite an enormous effort in pursuing un- or self-supervised deep learning techniques (Chen, 2024). In comparison, as shown in the various examples, the FKK sparse inversion method has gained industrial acceptance, and widely applied in commercial high-productivity activities both

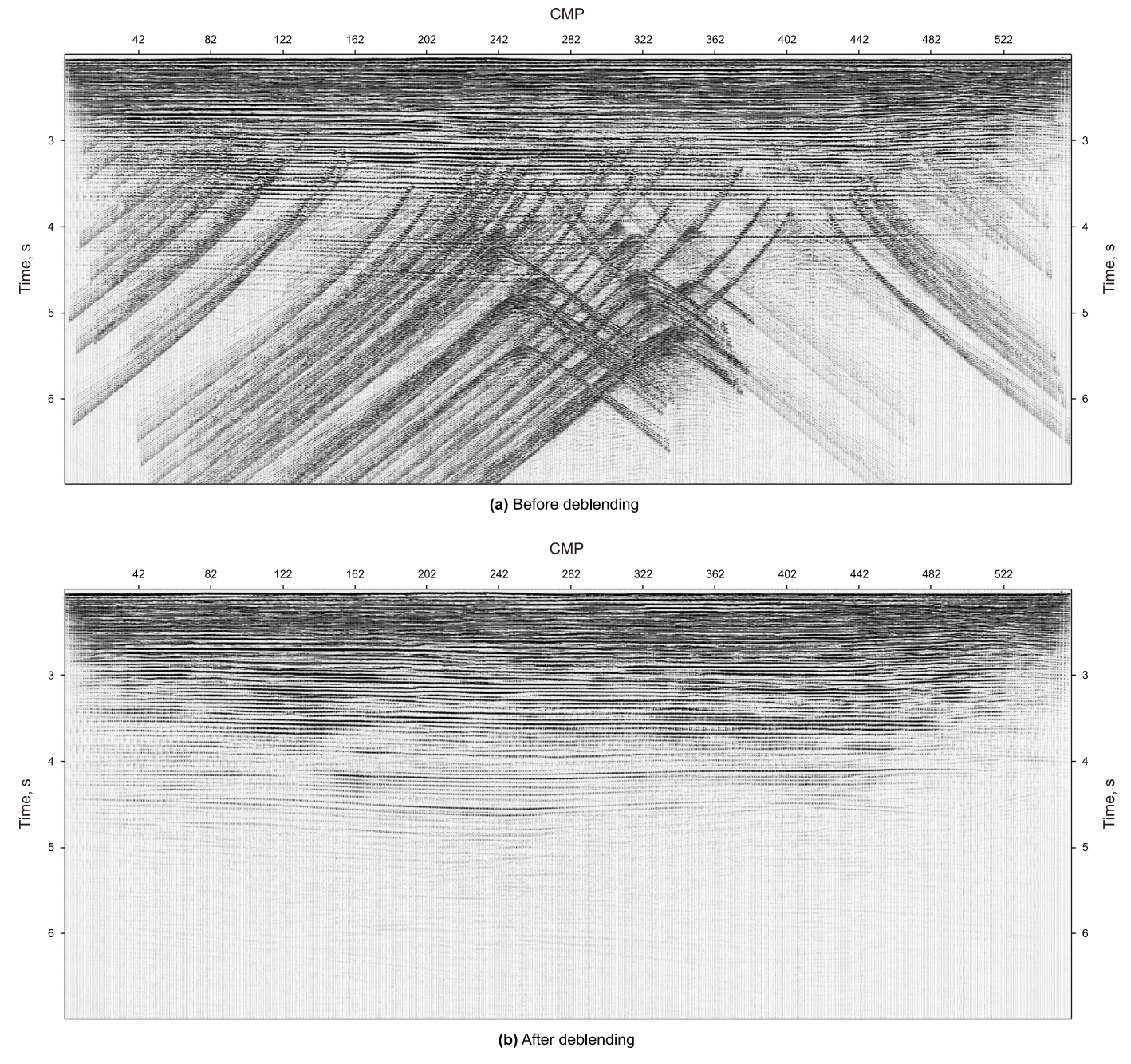


Fig. 16. Comparison of a stack section (a) before and (b) after deblending.

onshore and offshore cases.

At present, for hydrocarbon exploration in areas with complex surface conditions unsuitable for vibroseis, simultaneous shooting is only applied with sufficient time-distance separation that the wavefield is not blended. To further improve acquisition efficiency, it is necessary to reduce the time-distance separation to allow wavefield blended, and subsequently deblending techniques are required. To address this challenge, there is a need to develop deblending algorithms accounting for the characteristics of the deblending procedure due to complex near surface conditions. Note that multicomponent seismic is another effective tool for hydrocarbon exploration in complex areas (Li, 1997; Li and Zhang, 2011, 2021) and can also be benefit from blended acquisition to improve its cost-effectiveness.

6. Conclusions

In summary, we have reviewed the filtering, inversion and deep learning-based deblending techniques, and propose to use the FKK sparse inversion technique for deblending. Synthetic blended data deblending shows that its deblending error is less than 0.1% in average amplitudes, and less than -40db in amplitude spectra. The FKK sparse inversion technique has been widely applied in land, marine OBN and streamer data acquisition. In comparison, the filtering-based deblending techniques often fail in high-fold blended cases, and deep learning-based techniques require large training labels which are often unavailable in reality. Un- or self-supervised deep learning-based techniques appear to be a way forward in the near future. In a longer term, FWI imaging of

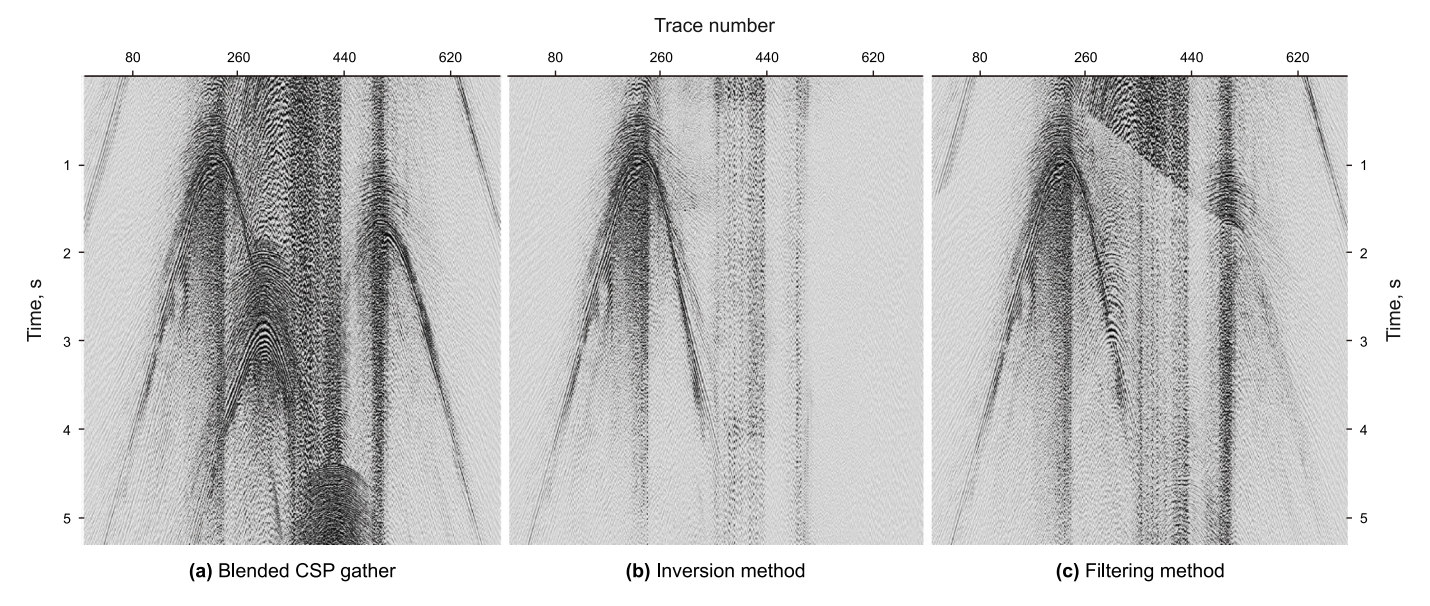


Fig. 17. Real data comparison: (a) pseudo-deblended data in CSP domain; deblended results by (b) the FKK sparse inversion (Song et al., 2019b) and (c) the traditional median filter method of Wang et al. (2014) for comparisons.

blended data without deblending may be a potential solution.

CRediT authorship contribution statement

Shao-Hua Zhang: Writing — review & editing, Validation, Supervision, Resources, Project administration, Funding acquisition, Conceptualization. **Jia-Wen Song:** Writing — original draft, Software, Methodology, Formal analysis.

Data availability

The data are available from the corresponding author upon reasonable request.

Declaration of competing interest

We hereby declare that there is no conflict of interest.

Acknowledgements

We thank BGP's project partners in the Middle East for permission to show the data. We thank Xiang-Yang Li for his comments on the manuscript. This work is supported by National Science and Technology Major Project (Grant No. 2017ZX05018–001).

References

Abma, R.L., Manning, T., Tanis, M., Yu, J., Foster, M., 2010. High quality separation of simultaneous sources by sparse inversion. In: 72nd EAGE Conference and Exhibition incorporating SPE EUROPEC 2010, cp-161-00019. https://doi.org/10. 3997/2214-4609.201400611.

Abma, R., Howe, D., Foster, M., Ahmed, I., Tanis, M., Zhang, Q., Arogunmati, A., Alexander, G., 2015. Independent simultaneous source acquisition and processing. Geophysics 80 (6), WD37–WD44. https://doi.org/10.1190/geo2015-0078.1.

Baardman, R.H., Hegge, R.F., 2020. Machine learning approaches for use in deblending. Lead. Edge 39 (3), 188–194. https://doi.org/10.1190/tle39030188.1. Beasley, C.J., 2008. A new look at marine simultaneous sources. Lead. Edge 27 (7), 914–917. https://doi.org/10.1190/1.2954033.

Berkhout, A.J., 2008. Changing the mindset in seismic data acquisition. Lead. Edge 27, 924–938. https://doi.org/10.1190/1.2954035.

Birnie, C., Alkhalifah, T., 2022. Transfer learning for self-supervised, blind-spot seismic denoising. Front. Earth Sci. 10, 1053279. https://doi.org/10.3389/

feart 2022 1053279

Blumensath, T., Davies, M.E., 2008. Iterative thresholding for saparse approximations. J. Fourier Anal. Appl. 14, 629–654. https://doi.org/10.1007/s00041-008-9035-z.

Bouska, J., 2008. Distance separated simultaneous sweeping: the world's fastest vibroseis technique. EAGE Vibroseis Workshop. https://doi.org/10.1111/j.1365-2478.2009.00843.x.

Cao, J., Verschuur, E., Gu, H., Li, L., 2019. Joint deblending and data reconstruction with focal transformation. Geophysics 84 (3), V219–V231. https://doi.org/ 10.1190/geo2018-0626.1.

Chen, X., 2024. Seismic Data Deblending Based on Self-Supervised Deep Learning. Master Thesis, Tongji University.

Chen, X., Wang, B., 2023. Self-supervised multistep seismic data deblending. Surv. Geophys. 1–25. https://doi.org/10.1007/s10712-023-09801-z.

Chen, Y., 2015. Iterative deblending with multiple constraints based on shaping regularization. Geosci. Rem. Sens. Lett. IEEE 12 (11), 2247–2251. https://doi.org/ 10.1109/lgrs.2015.2463815.

Chen, Y., Fomel, S., Hu, J., 2014. Iterative deblending of simultaneous source seismic data using seislet-domain shaping regularization. Geophysics 79 (5), V179–V189. https://doi.org/10.1190/geo2013-0449.1.

Cheng, J., Sacchi, M.D., 2015. A fast rank-reduction algorithm for 3D deblending via randomized QR decomposition. In: SEG Annual Meeting. Expanded Abstracts, pp. 3830–3835. https://doi.org/10.1190/segam2015-5850767.1.

Dai, W., Wang, X., Schuster, G.T., 2011. Least-squares migration of multisource data with a deblurring filter. Geophysics 76 (5), R135—R146. https://doi.org/10.1190/geo2010-0159.1.

Daubechies, I., Defrise, M., Mol, C.D., 2004. An iterative thresholding algorithm for linear inverse problems with a sparsity constraint. Commun. Pure Appl. Math. 57 (11), 1413–1457. https://doi.org/10.1002/cpa.20042.

Dong, L., Zhang, M., Luo, F., Zhang, Y., Wang, Z., Wei, G., 2021. Supressing blended noise by iterative inversion through singular value decomposition. Oil Geophys. Prospect. 56 (1), 57–61+116+117. https://doi.org/10.13810/j.cnki.issn.1000-7210.2021.01.006.

Doulgeris, P., Mahdad, A., Blacquiere, G., 2011. Iterative separation of blended marine data. discussion on the coherency-pass filter. SEG Tech. Progr. Expand. Abstr. 30 (1), 26–31. https://doi.org/10.1190/1.3627754.

Gan, S., Wang, S., Chen, Y., Chen, X., Xiang, K., 2016. Separation of simultaneous sources using a structural-oriented median filter in the flattened dimension. Comput. Geosci. 86, 46–54. https://doi.org/10.1016/j.cageo.2015.10.001.

Hampson, G., Stefani, J., Herkenhoff, F., 2008. Acquisition using simultaneous sources. Lead. Edge 27 (7), 918–923. https://doi.org/10.1190/1.2954034.

Han, L., Tan, C., Lv, Q., Zhang, Y., Gong, X., 2013. Separation of multi-source blended seismic acquisition data by iterative denoising. Chin. J. Geophys. 56 (7), 2402–2412. https://doi.org/10.6038/cjg20130726.

Howe, D., Foster, M., Allen, T., Jack, I., 2009. Independent Simultaneous Sweeping in Libya. Full scale implementation and new developments. In: 79th Annual International SEG Annual Meeting. Expanded Abstracts, pp. 109–111. https:// doi.org/10.1190/1.3255044.

Huo, S., Luo, Y., Kelamis, P.G., 2012. Simultaneous sources separation via multidirectional vector-median filtering. Geophysics 77 (4), V123–V131. https://doi.org/10.1190/geo2011-0254.1.

Ibrahim, A., Sacchi, M.D., 2014. Simultaneous source separation using a robust

- Radon transform. Geophysics 79 (1), V1–V11. https://doi.org/10.1190/geo2013-0168 1
- Laine, S., Karras, T., Lehtinen, J., Aila, T., 2019. High-quality self-supervised deep image denoising. Adv. Neural Inf. Process. Syst. 32. https://doi.org/10.48550/ arxiv.1901.10277.
- Li, P., Song, J., Zhang, S., Wang, W., Sun, P., Ma, Y., 2019. Deblending by sparse inversion: case study on land data from Oman. In: 89th Annual International SEG Meeting. Expanded Abstracts, pp. 97–101. https://doi.org/10.1190/ segam2019-3215362.1.
- Li, X.-Y., 1997. Fractured reservoir delineation using multicomponent seismic data. Geophys. Prospect. 45, 39–64. https://doi.org/10.1046/j.1365-2478.1997.3200262.x.
- Li, X.-Y., 1999. Fracture detection using azimuthal variation of P-wave moveout from orthogonal seismic survey lines. Geophysics 64 (4), 1193—1201. https://doi.org/10.1190/1.1444626.
- Li, X.-Y., Zhang, Y.-G., 2011. Seismic reservoir characterization: how can multicomponent data help? J. Geophys. Eng. 8 (2), 123–141. https://doi.org/10.1088/1742-2132/8/2/001.
- Li, X.-Y., Zhang, S., 2021. Forty years of shear-wave splitting in seismic exploration: an overview. Geophys. Prospect. Pet. 60 (2), 190–209. https://doi.org/10.3969/j.issn.1000-1441.2021.02.002 (in Chinese).
- Lin, R., Bahia, B., Sacchi, M.D., 2022. Iterative deblending of simultaneous-source seismic data via a robust singular spectrum analysis filter. IEEE Trans. Geosci. Rem. Sens. 60, 1–10. https://doi.org/10.1109/tgrs.2021.3086834.
- Liu, Y., Liu, C., Wang, D., 2009. A 1D time-varying median filter for seismic random, spike-like noise elimination. Geophysics 74 (1), V17–V24. https://doi.org/10.1190/1.3043446.
- Luiken, N., Ravasi, M., Birnie, C., 2023. Integrating self-supervised denoising in inversion-based seismic deblending. Geophysics 89 (1), WA39—WA51. https:// doi.org/10.1190/geo2023-0131.1.
- Lynn, H.B., Simon, K.M., Bates, C.R., 1996. Correlation between P-wave AVOA and S-wave traveltime anisotropy in a naturally fractured gas reservoir. Lead. Edge 15 (8), 931–935. https://doi.org/10.1190/1.1437394.
- (8), 931–935. https://doi.org/10.1190/1.1437394.

 Mahdad, A., Doulgeris, P., Blacquiere, G., 2011. Separation of blended data by iterative estimation and subtraction of blending interference noise. Geophysics 76 (3), Q9–Q17. https://doi.org/10.1190/1.3556597.
- Qu, S., Zhou, H., Liu, R., et al., 2016. Deblending of simultaneous source seismic data using fast iterative shrinkage thresholding algorithm with firm thresholding. Acta Geophys. 64 (4), 1064–1092. https://doi.org/10.1515/acgeo-2016-0043.
- Quigley, J., 2004. An integrated 3D acquisition and processing technique using point sources and point receivers. In: 72nd Annual International SEG Meeting, Expanded Abstracts 21. https://doi.org/10.1190/1.1839677.
- Rozemond, H.J., 1996. Slip-sweep acquisition. In: 66th Annual International SEG Meeting. Expanded Abstracts, pp. 64–67. https://doi.org/10.1190/1.1826730.
- Song, J., Li, P., Wang, W., Wang, C., Li, H., Wang, B., 2019a. Separation of high-productivity blended seismic data based on sparse inversion. Oil Geophys. Prospect. 54 (2), 268–273. https://doi.org/10.13810/j.cnki.issn.1000-7210.2019.02.004.
- Song, J., Li, P., Qian, Z., Zhang, M., Sun, P., Wang, W., Ma, Y., 2019b. Simultaneous vibroseis data separation through sparse inversion. Lead. Edge 38 (8), 625–629. https://doi.org/10.1190/tle38080625.1.
- Song, J., Li, P., Sun, P., Ding, G., Yan, W., Chen, Y., Zhang, X., 2020. Deblending of simultaneous OBN data via sparse inversion. In: 90th Annual International SEG Meeting. Expanded Abstracts, pp. 106–110. https://doi.org/10.1190/segam2020-34259371.
- Sun, J., Slang, S., Elboth, T., Larsen, Greiner T., McDonald, S., Gelius, L.-J., 2020. A convolutional neural network approach to deblending seismic data. Geophysics 85 (4), WA13–WA26. https://doi.org/10.1190/geo2019-0173.1.
- Vermeer, G.J.O., 2002. 3D seismic survey design. Society of Exploration Geophysicists, New York.
- Verschuur, D., Berkhout, A., 2011. Seismic migration of blended shot records with surface-related multiple scattering. Geophysics 76 (1), A7—A13. https://doi.org/ 10.1190/1.3521658.

- Wang, B., Li, J., Han, D., 2022. Iterative deblending using MultiResUNet with multilevel blending noise for training and transfer learning. Geophysics 87 (3), V205–V214. https://doi.org/10.1190/geo2021-0341.1.
- Wang, B., Li, J., Luo, J., Wang, Y., Geng, J., 2021. Intelligent deblending of seismic data based on U-Net and transfer learning. IEEE Trans. Geosci. Rem. Sens. 59 (10), 8885–8894. https://doi.org/10.1109/tgrs.2020.3048746.
- Wang, B., Lin, S., Chen, X., 2024. Self-supervised simultaneous deblending and interpolation of incomplete blended data using a multistep blind-trace U-Net. Pet. Sci. 22 (3), 1098–1109. https://doi.org/10.1016/j.petsci.2024.12.023.
- Wang, K., Hu, T., Wang, S., 2023a. Iterative deblending using unsupervised learning with double-deep neural networks. Geophysics 88 (3), V187–V205. https:// doi.org/10.1190/geo2022-0299.1.
- Wang, S., Hu, W., Yuan, P., Wu, X., Zhang, Q., Nadukandi, P., Botero, G.O., Chen, J., 2023b. A self-supervised deep learning method for seismic data deblending using a blind-trace network. IEEE Transact. Neural Networks Learn. Syst. 34 (7), 3405–3414. https://doi.org/10.1109/tnnls.2022.3188915.
- Wang, W., Li, H., Zhao, B., Luo, G., Zhang, X., Guo, H., 2014. Cross interference noise attenuation using alpha-trimmed vector median filtering. In: 76th EAGE Conference and Exhibition 2014, T08. https://doi.org/10.3997/2214-4609.20141584.
- Wilson, I.-J., Jarred, H., Rajiv, K., Wouter, G.B., Saeeda, H., Yousif, I.K.A., 2023. Deblending seismic data using multistage iterative source separation with priors-A case study using streamer 3D data. In: SEG International Exposition and Annual Meeting. SEG-2023-3909416. https://doi.org/10.1190/image2023-3909416.1
- Xu, W., Lipari, V., Bestagini, P., Ravasi, M., Chen, W., Tubaro, S., 2022. Intelligent seismic deblending through deep preconditioner. Geosci. Rem. Sens. Lett. IEEE 19, 1–5. https://doi.org/10.1109/lgrs.2022.3193716.
- Zhang, C., Olofsson, B., 2012. Separating simultaneous source data using weighted tau-p transform. In: EAGE Extended Abstracts, pp. 1–5. https://doi.org/10.3997/ 2214-4609.20148371.
- Zhang, Q., Mao, W., Zhou, H., Zhang, H., Chen, Y., 2018. Hybrid-domain simultaneous-source full waveform inversion without crosstalk noise. Geophys. J. Int. 215 (3), 1659–1681. https://doi.org/10.1093/gji/ggy366.
- Zhang, S., Song, Q., 2025. Reservoir characterization: how broadband wide-azimuth and high density seismic can help. J. Geophys. Eng. 22 (1), 221–237. https://doi.org/10.1093/jge/gxae128.
- Zhang, S., Zhan, S., 2021. Broadband Wide-Azimuth and High-Density Seismic Technology. Petroleum Industry Press, Beijing.
- Zhao, J., Zhu, J., Yasin, C., Clow, F., 2018. Vibroseis ultra high productivity blended acquisition: field trial and full scale implementation in Oman. In: 2018 CPS/SEG International Geophysical Conference, pp. 150–153. https://doi.org/10.1190/igc2018-038.
- Zhou, L., Zhuang, Z., Cheng, J., 2016a. Multi-source blended wavefield separation for marine seismic based on an adaptive iterative multi-level median filtering. Oil Geophys. Prospect. 51 (3), 434–443. https://doi.org/10.13810/j.cnki.issn.1000-7210.2016.03.003.
- Zhou, Y., Gao, J., Chen, W., Frossard, P., 2016b. Seismic simultaneous source separation via patchwise sparse representation. IEEE Trans. Geosci. Rem. Sens. 54 (9), 5271–5284. https://doi.org/10.1109/tgrs.2016.2559514.
- Zhou, Y., Li, S., 2018. Simultaneous deblending and interpolation using structure-oriented filters. J. Appl. Geophys. 150, 230–243. https://doi.org/10.1016/j.jappgeo.2018.01.015.
- Zhou, Z., Zhang, Y., Zhang, M., Zhou, H.-W., 2013. Separation of ISS Seismic Data via Vector Median Filter in T-X and F-X Domains. Society of Exploration Geophysicists. https://doi.org/10.1190/segam2013-0344.1.
- Zu, S., Cao, J., Qu, S., Chen, Y., 2020. Iterative deblending for simultaneous source data using the deep neural network. Geophysics 85 (2), V131–V141. https:// doi.org/10.1190/geo2019-0319.1.
- Zu, S., Zhou, H., Wu, R., Mao, W., Chen, Y., 2018. Hybrid-sparsity constrained dictionary learning for iterative deblending of extremely noisy simultaneous-source data. IEEE Trans. Geosci. Rem. Sens. 57 (4), 2249–2262. https://doi.org/10.1109/tgrs.2018.2872416.